Available online at www.sciencedirect.com
ScienceDirect
Trans. Nonferrous Met. Soc. China 30(2020) 2967−2979
Transactions of Nonferrous Metals Society of China
www.tnmsc.cn

Corrosion resistance of Mg−Al LDH/$Mg(OH)_2$/silane−Ce hybrid coating on magnesium alloy AZ31

Zai-meng QIU[1], Rong-chang ZENG[1,2], Fen ZHANG[1], Liang SONG[1], Shuo-qi LI[1]

1. Corrosion Laboratory for Light Metals, College of Materials Science and Engineering, Shandong University of Science and Technology, Qingdao 266590, China;
2. School of Materials Science and Engineering, Zhengzhou University, Zhengzhou 450002, China

Received 11 February 2020; accepted 17 July 2020

Abstract: An environmentally-friendly hybrid coating on AZ31 magnesium alloy substrates was reported. The synergic effect was studied on Mg−Al-layered double hydroxide Mg−Al LDH/$Mg(OH)_2$-coated AZ31 magnesium alloy via an in-situ steam coating process and a subsequent combined surface modification of bis-[triethoxysilylpropyl]tetrasulfide (BTESPT) silane and $Ce(NO_3)_3$. The microstructure and composition characteristics of the hybrid coatings were investigated by means of X-ray diffraction (XRD), scanning electronic microscopy (SEM), Fourier transform infrared spectrophotometry (FT-IR) and X-ray photoelectron spectroscopy (XPS). The corrosion resistance of the coated samples was evaluated by potentiodynamic polarization (PDP), electrochemical impedance spectrum (EIS) and hydrogen evolution rate during immersion in 3.5 wt.% NaCl solution. The results show an improved corrosion resistance of the alloy in the presence of BTESPT silane and $Ce(NO_3)_3$. This is most likely due to the synergistic effect of steam coating and silane coating to enhance the barrier properties of hybrid coating. In addition, the formation mechanism and anti-corrosion mechanism of coatings were discussed.
Key words: magnesium alloy; silane coating; layered double hydroxide; corrosion resistance

1 Introduction

Magnesium alloys have significant advantages over other alloys, such as low density, high stiffness/mass ratios, good vibration and good cast ability [1−3]. Unfortunately, magnesium alloys are very susceptible to corrosion due to their high chemical activity which restricted their use on a large scale [4−6]. At present, various methods have been used to protect magnesium alloys, including chemical conversion [7,8], micro-arc oxidation (MAO) [9,10], polymeric coatings [11,12], and electrochemical plating [13,14].

Layered double hydroxides (LDHs) have good properties, such as flame retardant performance, high efficiency adsorption and adjustable elemental composition. This kind of inorganic nano-container is small in size, large in load and easy to be modified, so it is widely used in corrosion protection research [15−18]. In addition, LDHs have the unique feature of ion-exchange, which rendered LDHs to be widely used as coatings to provide protection for magnesium alloys [19,20]. Various methods of preparing LDHs coatings have been proposed. YE et al [21] prepared the NiAl−LDH on Mg alloy by a simple one-step hydrothermal method. WU et al [22] fabricated Mg−M LDH on anodized AZ31 magnesium alloy by a facile in-situ growth method. In the previous

Foundation item: Projects (51601108, 21676285, 51571134) supported by the National Natural Science Foundation of China; Project (2017RCJJ015) supported by Scientific Research Foundation of Shandong University of Science and Technology for Recruited Talents, China; Project (2014TDJH104) supported by the Shandong University of Science and Technology Research Fund, China
Corresponding author: Fen ZHANG; Tel: +86-15966800553; E-mail: zhangfen2011@hotmail.com
DOI: 10.1016/S1003-6326(20)65435-8

studies, our research group reported some methods for preparing LDH coatings on Mg and Al alloys surfaces to improve corrosion resistance [23−25]. Recently, an in-situ steam growth coating has been developed to improve the corrosion resistance without any chemical pretreatment [26,27]. The LDH/$Mg(OH)_2$ coatings were obtained on the surface of the magnesium alloy in a closed high-pressure reaction autoclave with ultrapure water [28]. However, there are many pore holes in the steam coating (SC), which would increase the opportunity for penetration of the aggressive medium to the metal substrate. Therefore, a post-sealing process is necessarily required to improve the corrosion protection of the steam coating.

Currently, the silane coating is considered to be an effective method to improve the corrosion resistance of magnesium alloys [29−31]. The good barrier properties of the silane coatings are due to the development of a dense —Si—O—Si— network, which hinders the penetration of aggressive species towards metallic substrate [32]. Thus, the effectiveness of the silane coatings is strongly dependent on the barrier properties of the coating. In order to obtain enhanced anti-corrosion behaviour, the improvement of the barrier property of the coating is an important aim. The silane coating also has many small defects such as pinholes or cracks, which leads to the onset and acceleration of corrosion. On the other hand, in order to improve the protective properties of the silane coating, the corrosion inhibitor is directly doped in the silane coatings. Research showed that cerium salt is an excellent corrosion inhibitor [33]. The addition of a small amount of rare earth ions can promote the hydrolysis and agglomeration of silane [34]. This procedure aims at improving the barrier property of silane coating by adding cerium ions and improving the corrosion resistance of hybrid coating.

In this work, anti-corrosion hybrid coatings on magnesium alloy were prepared. Firstly, a steam coating was prepared on magnesium alloy by a simple in-situ steam growth method, which can greatly shorten the preparation cycle. Subsequently, the bis-[triethoxysilylpropyl]tetrasulfide (BTESPT)/Ce^{3+} modified coatings were prepared by a one-step dipping process. BTESPT is a multi-functional silane coupling agent that can form six hydrolysable silanol groups, which would facilitate the reaction with the metallic substrates.

In order to give a comprehensive evaluation of the potential application of this new coating, electrochemical properties as well as the early deterioration of the hybrid coatings during immersion in NaCl solution were investigated and correlated with the microstructure of the coating.

2 Experimental

2.1 Formation of hybrid coatings on AZ31 alloys

Figure 1 illustrates the schematic representation of the preparation process of the hybrid coatings on the Mg alloy. AZ31 Mg alloy (3.0 wt.% Al, 1.0 wt.% Zn and balanced Mg) specimens (Shandong Yuyuan Light Metal Precise Forming Co., Ltd., China) with dimensions of 20 mm × 20 mm × 5 mm were used as substrate materials. The substrate was ground to 2500 grit with SiC paper, then cleaned with ethanol and dried in the air.

Firstly, 20 mL of pure water was added to the bottom of a 100 mL Teflon-lined autoclave to generate steam. The AZ31 alloy was placed in the autoclave with a cotton thread to maintain a distance of 3 cm between the AZ31 substrate and water surface. The autoclave was heated to 433 K for 6 h and cooled naturally to room temperature. After steam treatment, the sample was washed with ethanol and dried with hot air.

Secondly, the BTESPT silane (Jingke Chemical Reagent Co., Ltd., China) Solution 1 (4 vol.% silane, 96 vol.% methanol) was prepared and solution 2 (4 vol.% silane, 90 vol.% methanol, 6 vol.% $Ce(NO_3)_3$ solution) was obtained by adding 1×10^{-3} mol/L of $Ce(NO_3)_3$. Then, the silane/Ce mixed solutions were stirred for 1 h and placed for 3 d. Finally, the Mg−Al LDH/$Mg(OH)_2$-coated AZ31 magnesium alloys were immersed once in the prepared silane solutions for 30 s and then cured in a drying oven at 120 °C for 30 min. The samples prepared with the above two different silane solutions were designated as SC/BTESPT coating and SC/BTESPT/Ce^{3+} coating, respectively.

2.2 Surface characterization

Surface morphologies of the obtained coatings were observed using field-emission scanning electron microscopy (FE-SEM, Nova NanoSEM 450,

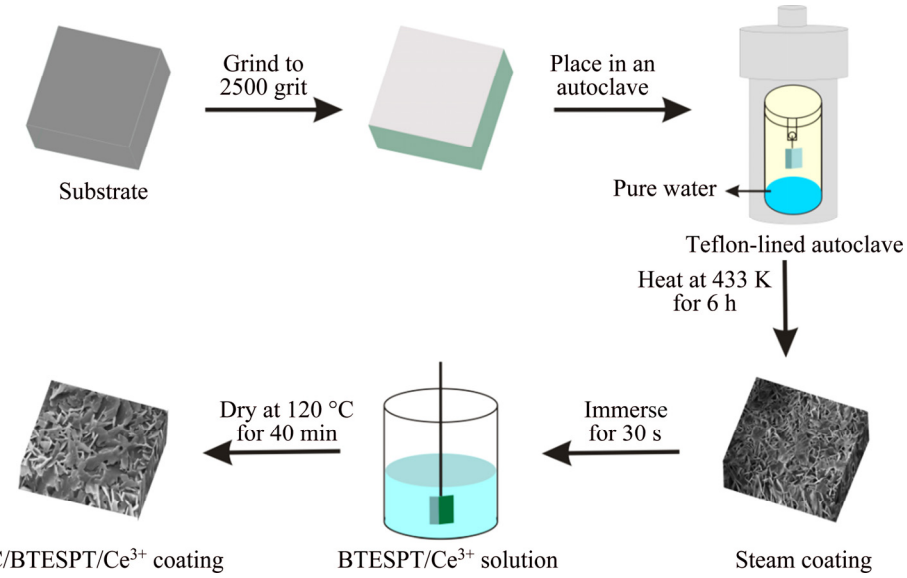

Fig. 1 Schematic diagram of preparation process of hybrid coatings

USA). The composition of element was determined by equipped energy dispersive X-ray spectrometer (EDS). The chemical bonds in the coating were characterized by Fourier transform infrared spectrophotometer (FTIR, Nicolet 380, Thermo Electron Corporation, USA). The crystal micro-structure of the coatings was analyzed by X-ray diffractometer (XRD, Rigaku D/MAX2500PC, Japan).

2.3 Corrosion characterization

The corrosion properties were evaluated via an electrochemical Princeton potentiostat (PARSTAT2273, Princeton Instruments Corporation, USA) apparatus equipped with a classical three-electrode cell, consisting of the specimen with an exposed area of 1 cm^2 as the working electrode, saturated calomel as the reference electrode and the platinum as counter electrode. All experiments were conducted in 3.5 wt.% NaCl solution at room temperature. The EIS measurements on the samples were carried out at their open-circuit potential (OCP) with a peak-to-peak amplitude of 10 mV in the frequency range from 100 kHz to 10 mHz. Potentiodynamic polarization (PDP) measurement was performed by scanning the potential from −2.0 to −0.5 V with respect to the OCP value at a scan rate of 1 mV/s. The results were fitted to the equivalent circuit model and analyzed by ZSimpWin software.

3 Results

3.1 Microstructure and chemical compositions of coatings

Figure 2 demonstrates the SEM morphologies of the steam coating and hybrid coatings. Figure 2(a) shows that the obtained coating is dense on the entire magnesium alloy substrate. Figure 2(b) provides a high magnification image of the steam coating, demonstrating that the coating consisted of uniform nano-plates that grew roughly vertically on the substrate. As observed, the elemental compositions (Point 1 and Point 2) illustrate that the steam coating is mainly composed of O, Mg, Al and C, indicating the presence of Mg−Al LDH and $Mg(OH)_2$. It is noted that there are similarities in morphology between the SC/BTESPT (Fig. 2(c)), SC/BTESPT/Ce^{3+} coatings (Fig. 2(d)) and the steam coating. Compared with steam coating, the surface of the hybrid coating appeared to be smoother. In view of the presence of the BTESPT, the hybrid coatings may be covered by a layer of oily substance. The EDS analysis shows that BTESPT modified coatings (Points 3−6) are composed of O, Mg, Al, C, S and Si elements. Particularly, the SC/BTESPT/ Ce^{3+} coating (Points 5 and 6) is also composed of a small amount of Ce element (see Table 1).

The cross-sectional morphology of the SC/BTESPT/Ce^{3+} coating is represented in Fig. 3(a).

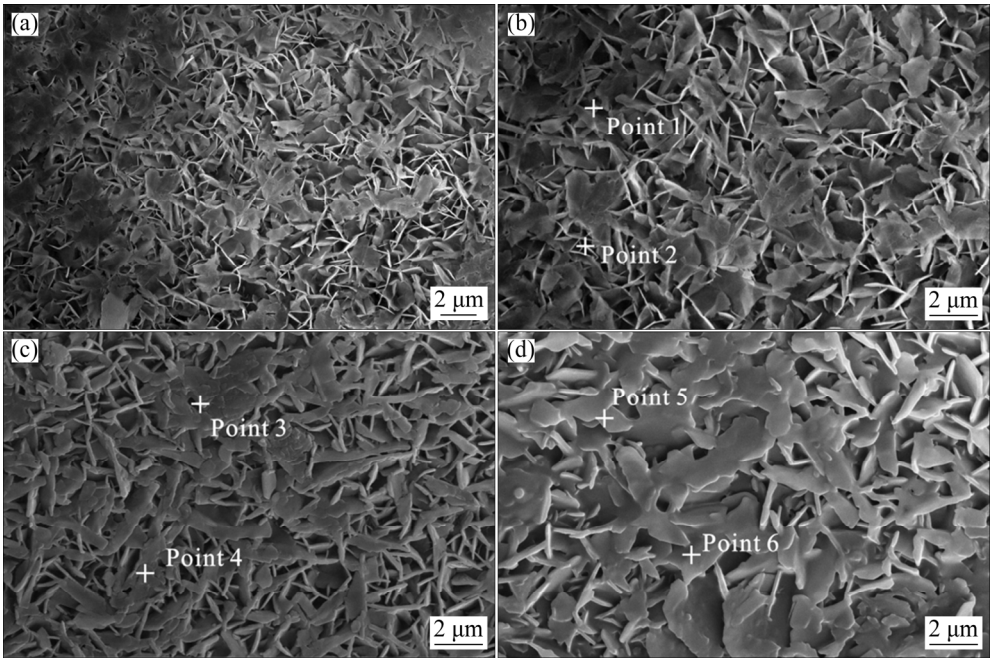

Fig. 2 SEM images of steam coating (a, b), SC/BTESPT coating (c) and SC/BTESPT/Ce^{3+} coating (d)

Table 1 Elemental compositions of coatings in Fig. 2 (wt.%)

Point	Mg	O	Al	C	S	Si	Ce	Total
1	55.39	40.43	2.05	2.13	−	−	−	100
2	55.61	40.14	1.99	2.21	−	−	−	100
3	21.42	47.74	1.42	16.47	8.65	4.31	−	100
4	23.47	44.97	1.92	11.95	11.41	6.28	−	100
5	21.45	39.65	1.31	17.50	12.85	6.85	0.38	100
6	19.48	41.48	1.46	20.53	11.04	5.26	0.34	100

The EDS mappings are shown in Figs. 3(b)−(f). Figure 3(a) shows that the thickness of the steam coating is about (25±10) μm. As observed, the structure of steam coating is dense and uniform, and the thickness of BTESPT/Ce^{3+} layer is almost negligible, which may be due to the thin BTESPT/Ce^{3+} layer and the low accuracy of the instrument. The existence of BTESPT/Ce^{3+} will be proved in the subsequent FT-IR and XPS results.

The phase compositions of the coatings on the AZ31 alloy were analyzed by XRD. The structure and composition of the coating were confirmed. Figure 4(a) presents the characteristic peaks of AZ31 magnesium phase. As can be seen from Fig. 4(b), the pattern of the steam coating is clearly reflected, indicating that the LDH phase forms a good layered crystalline structure. The two peaks located at approximately 2θ=11.3° and 22.6° and can be distributed to (003) and (006) diffraction peaks, which are $[Mg_{1-x}Al_x(OH)_2(CO_3)_{x/2}]\cdot nH_2O$ (Mg−Al LDH) [35,36]. Meanwhile, Figs. 4(b−d) show the characteristic peaks of $Mg(OH)_2$ at 2θ=18.4°, 37.9° and 58.6°, indicating the formation of $Mg(OH)_2$ on the magnesium alloy. It is worth noting that the XRD patterns of the hybrid coatings (Figs. 4(c, d)) remain the same as those of the steam coating and no new peaks appear for the hybrid coating.

The steam coating, SC/BTESPT coating and SC/BTESPT/Ce^{3+}coating were assessed by FT-IR spectra, as shown in Fig. 5. The peak at 3469 cm^{-1} corresponds to O—H due to the presence of the water and the peak at 1633 cm^{-1} is attributed to the hydroxyl deformation mode of water (H_2O) [37]. The peak at 459 cm^{-1} corresponds to the vibrational mode of the Mg—O octahedron. The peak at 3694 cm^{-1} corresponds to the Mg—O—H stretching vibration of Mg−Al LDH and the peak at

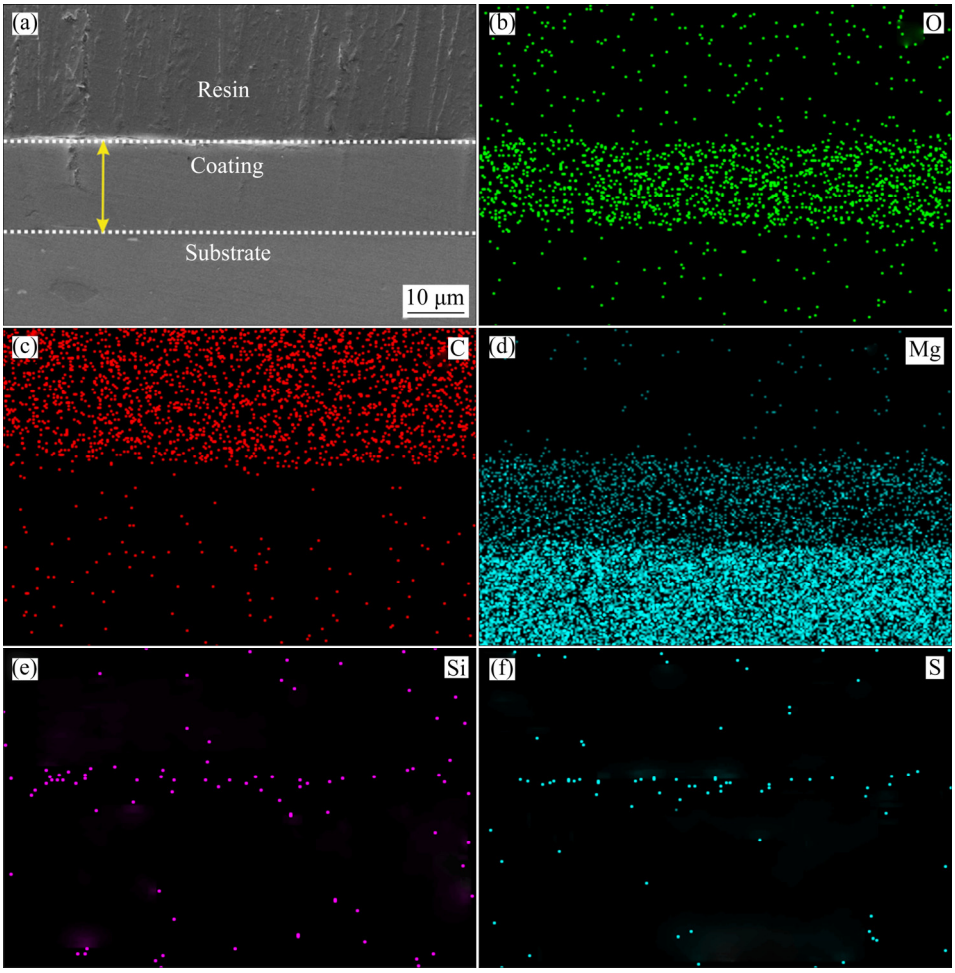

Fig. 3 Cross-sectional morphology of SC/BTESPT/Ce^{3+} coating (a) and corresponding EDS mapping images (b−f)

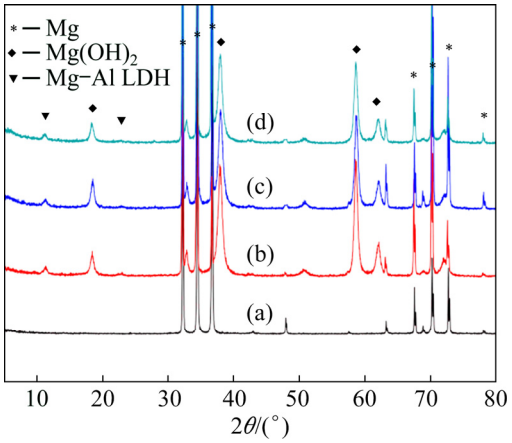

Fig. 4 XRD patterns of AZ31 alloy (a), steam coating (b), SC/BTESPT (c) and SC/BTESPT/Ce^{3+} (d) coatings

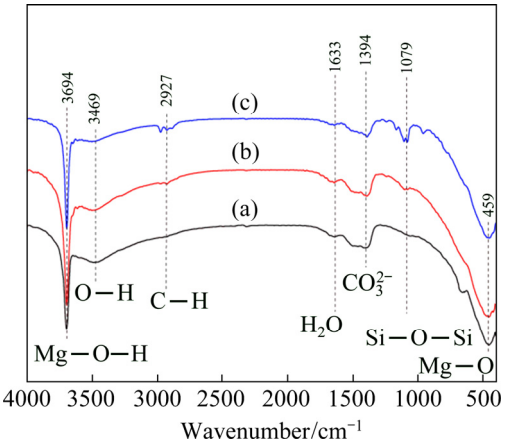

Fig. 5 FT-IR spectra of steam coating (a), SC/BTESPT coating (b) and SC/BTESPT/Ce^{3+} coating (c)

1394 cm^{-1} is assigned to the tensile vibration of the interlayer CO_3^{2-} [22]. Consequently, LDH is successfully generated via such an in-situ steam growth method on AZ31 alloys, which is in accordance with the XRD results as shown in Fig. 4. Additionally, the peak at about 2927 cm^{-1} belongs to C — H asymmetric and symmetric stretching vibrations, respectively [38]. The peak of Si — O — Si from BTESPT appears at 1079 cm^{-1} [39]. Based on the results, it is demonstrated that the hybrid silane coating was synthesized successfully.

The bonding structure of the SC/BTESPT/Ce^{3+}coating was characterized by XPS. Figure 6(a) shows that C 1s, O 1s and Si 2p signals can be observed in the survey spectra. This confirms the existence and combination of LDH and BTESPT in the hybrid coating. Figure 6(b) shows the C 1s spectra, which are C—H (284.6 eV), C—S (285.1 eV) and C—O (286.4 eV). Figure 6(c) shows the O 1s spectra, consisting of C—O, Mg—O—Si and Si—O—Si, which were centered at 531.7, 532.1 and 532.6 eV [40]. Figure 6(d) shows the Si 2p spectrum with three peaks of 101.6, 102.1 and 102.5 eV, corresponding to Si—C, Si—O—Si and Mg—O—Si, respectively [41]. It is worth noting that the Ce signal is not detected in the XPS, which may be due to the small amount of $Ce(NO_3)_3$ (6×10^{-5} mol/L) in the experiment. XPS analysis shows that the hybrid coating is formed on the surface of the AZ31 alloy and it is bonded by Mg—O—Si and Si—O—Si.

3.2 Corrosion resistance

Figure 7 compares the potentiodynamic polarization (PDP) curves for the samples. Table 2 lists values related to the estimation of the corrosion parameters for all coatings. Generally speaking, the higher corrosion potential or lower corrosion current density indicates lower corrosion rate and better corrosion resistance. As can be seen, the corrosion potential of all treated samples was higher than that of untreated alloys. The corresponding free-corrosion potentials (φ_{corr}) of AZ31 substrate and steam coating are −1.457 and −1.384 V, respectively. However, the φ_{corr} of SC/BTESPT coating and SC/BTESPT/Ce^{3+} coating are −1.364 and −1.293 V, which are more positive than that of the AZ31 substrate. Moreover, the corrosion current densities (J_{corr}) of the AZ31 alloy substrate is 1.296×10^{-5} A/cm^2 which is the highest compared with the coated samples, indicating that the substrate is easily to be corroded. The value of the steam coating sample is 1.923×10^{-7} A/cm^2 while those of the SC/BTESPT coating and SC/BTESPT/Ce^{3+} coating are 3.989×10^{-8} and 2.712×10^{-8} A/cm^2, respectively. In summary, the J_{corr} for the hybrid coating sample decreases by three orders of magnitude compared with that of AZ31 substrate. In addition, the polarization

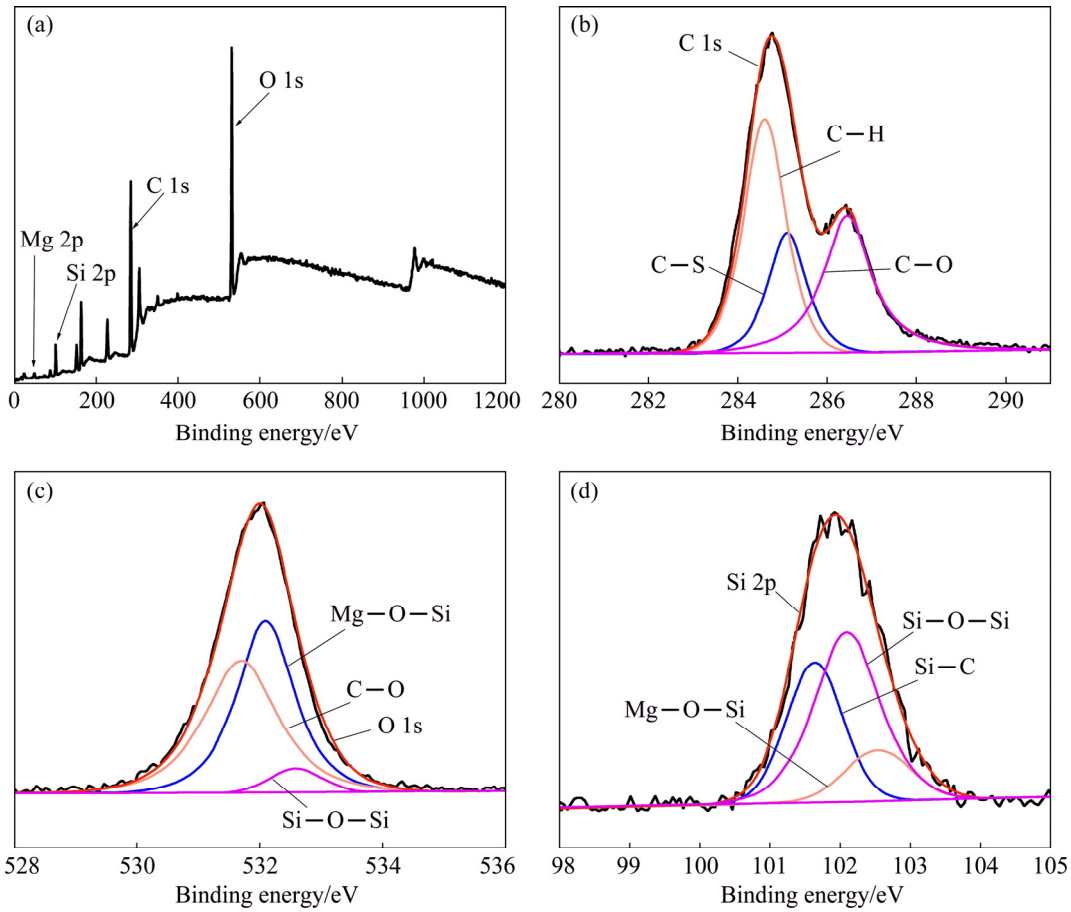

Fig. 6 XPS results of survey spectra (a), C 1s (b), O 1s (c) and Si 2p (d) of SC/BTESPT/Ce^{3+}coating

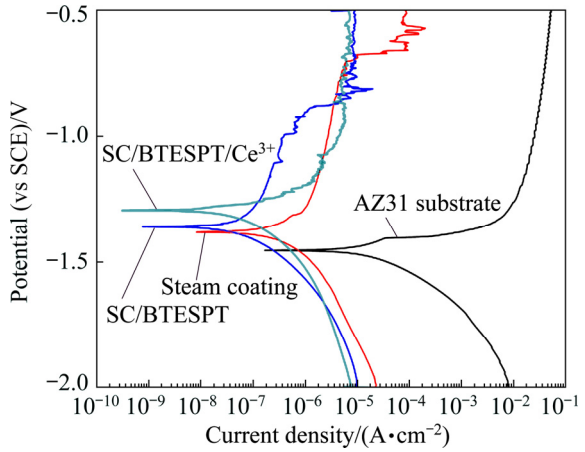

Fig. 7 PDP curves of as-prepared samples in 3.5 wt.% NaCl solution

resistance (R_p) of the different specimens increases in the following order: AZ31 substrate < steam coating < SC/BTESPT coating < SC/BTESPT/Ce^{3+} coating. Therefore, the SC/BTESPT/Ce^{3+} coating possesses the best corrosion resistance among all samples. It is worth noting that there are many breakdown potentials and passivation regions in the anodic branch of polarization curve for the coating. Such phenomenon is owing to the self-healing ability of LDH [23,42].

Electrochemical impedance spectrum (EIS) provides a powerful way to interpret the dynamics of the corrosion process. Figure 8(a) shows the Bode plots of different coatings in 3.5 wt.% NaCl solution. As is known to all, at lower frequencies, higher $|Z|$ modulus represents better corrosion resistance of metal substrate. It can be seen from Bode diagram that the impedance of SC/BTESPT/Ce^{3+} coating is the highest at the low frequency among different samples. Meanwhile, the Nyquist diagrams (Figs. 8(b, c)) present a capacitive semicircle in high frequency region and a slanted release line in low frequency region. Moreover, the SC/BTESPT/Ce^{3+} coating has a maximum radius of curvature, indicating that the sample has the highest corrosion resistance, which is owing to barrier properties of LDH and BTESPT.

Figures 8(d−f) show different equivalent circuit (EC) modes to fit the EIS results. The fitting data are listed in Table 3. For AZ31 substrate, the equivalent circuit (Fig. 8(d)) was proposed as R_s(CPE(R_{ct}($R_L L$))), where R_s represents the NaCl

Table 2 Electrochemical parameters of polarization curves of samples in Fig. 7

Sample	β_a/(mV·dec^{-1})	$-\beta_c$/(mV·dec^{-1})	φ_{corr}(vs SCE)/V	J_{corr}/(A·cm^{-2})	R_p/(Ω·cm^2)
AZ31 substrate	122.058	100.651	−1.457	1.296×10^{-5}	1.923×10^{4}
Steam coating	286.647	170.849	−1.384	1.923×10^{-7}	9.550×10^{5}
SC/BTESPT coating	363.771	278.319	−1.364	3.989×10^{-8}	1.290×10^{7}
SC/BTESPT/Ce^{3+} coating	358.469	426.550	−1.293	2.712×10^{-8}	3.596×10^{7}

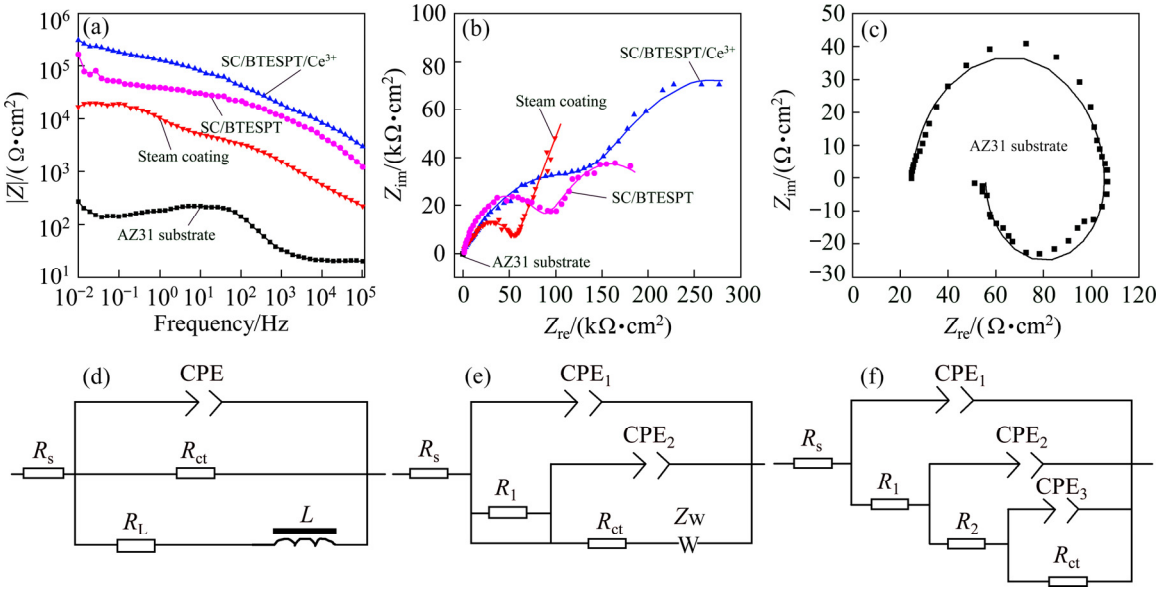

Fig. 8 EIS (a−c) and equivalent circuits of AZ31 substrate (d), steam coating (e), SC/BTESPT coating and SC/BTESPT/Ce^{3+} coating (f)

solution resistance, R_{ct} represents charge transfer resistance, L is the inductance, R_L is a low frequency resistor due to pitting and peeling of corrosion products. While for steam coating (Fig. 8(e)), a different model was applied as: $R_s(CPE_1(R_1(CPE_2(R_{ct}Z_w))))$, where R_1 designates steam coating resistance, Z_w represents the diffusion resistance of LDH, indicating that steam coating has the ability of ion-exchange. After modification with BTESPT and Ce^{3+}, the SC/BTESPT and SC/BTESPT/Ce^{3+} coatings have similar results and can be fitted with an EC (Fig. 8(f)): $R_s(CPE_1(R_1(CPE_2(R_2(CPE_3(R_{ct}))))))$, where R_2 designates hybrid coating resistance. Generally speaking, the higher the R_{ct} value, the better the corrosion resistance of the coating. As can be seen from Table 3, the R_{ct} value of SC/BTESPT/Ce^{3+} coating is the largest, so that it has the best corrosion resistance.

Figure 9 estimates the corrosion rate of the studied samples by continuously collecting hydrogen evolution volumes (HEVs) and hydrogen evolution rates (HERs). As can be seen in Figs. 9(a, a′), the HEVs of the steam coating and hybrid coatings are greatly reduced throughout the immersion time and the SC/BTESPT/Ce^{3+} coating

Table 3 EIS data recorded in Fig. 8

Sample	R_s/ ($\Omega\cdot cm^2$)	CPE_1/ ($\Omega^{-1}\cdot S^n\cdot cm^{-2}$)	R_{ct}/ ($\Omega\cdot cm^2$)	R_L/ ($\Omega\cdot cm^2$)	L/ ($H\cdot cm^{-2}$)	CPE_2/ ($\Omega^{-1}\cdot S^n\cdot cm^{-2}$)	CPE_3/ ($\Omega^{-1}\cdot S^n\cdot cm^{-2}$)	R_1/ ($\Omega\cdot cm^2$)	R_2/ ($\Omega\cdot cm^2$)	Z_w/ ($\Omega^{-0.5}\cdot S^{-1}\cdot m^{-2}$)
Substrate	22.09	1.497×10^{-5}	157.8	155.8	200.3	–	–	–	–	–
Steam coating	24.56	8.127×10^{-7}	5.520×10^{4}	–	–	6.397×10^{-7}	–	6080	–	3.134×10^{-5}
SC/ BTESPT	48.30	3.657×10^{-7}	9.299×10^{4}	–	–	2.079×10^{-5}	3.776×10^{-9}	1.244×10^{4}	1.420×10^{4}	–
SC/ BTESPT/ Ce^{3+}	51.32	1.272×10^{-6}	2.507×10^{5}	–	–	1.778×10^{-5}	8.729×10^{-10}	1.680×10^{5}	2.507×10^{5}	–

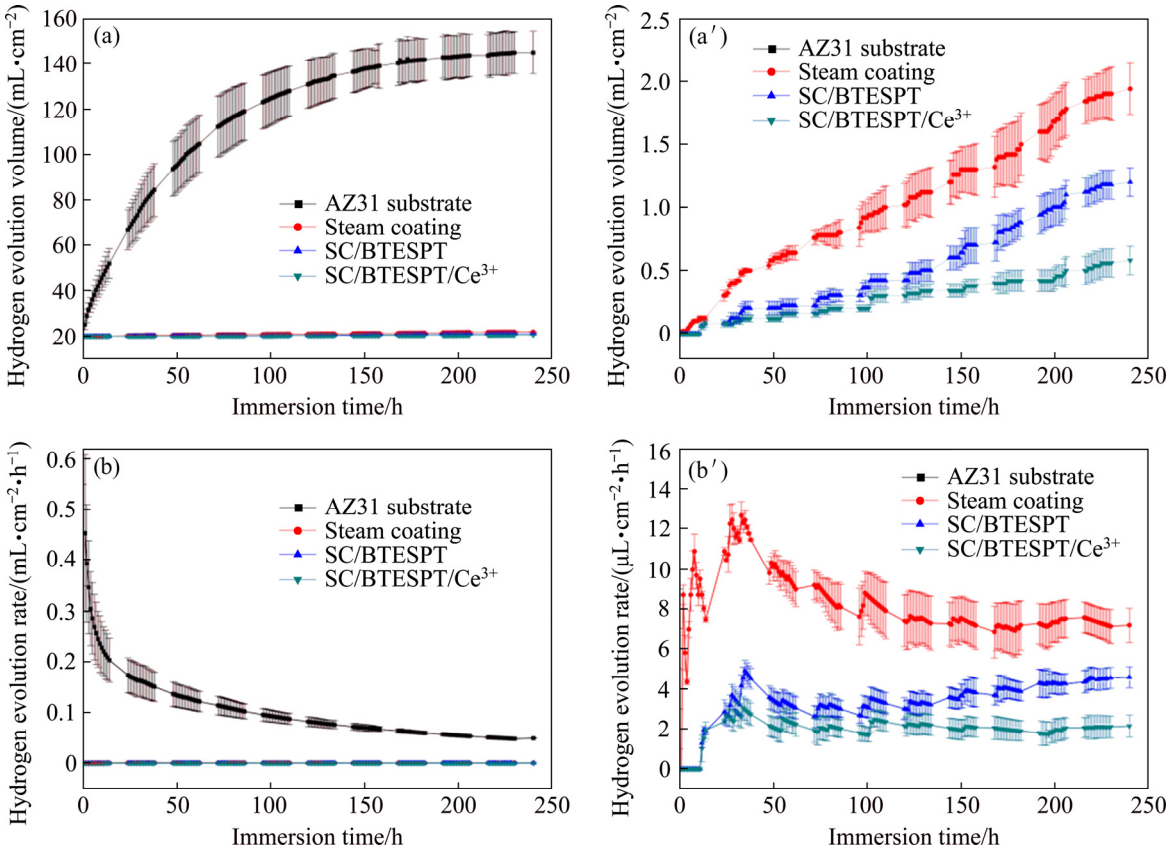

Fig. 9 Function of hydrogen evolution volume (a, a′) and hydrogen evolution rate (b, b′) of AZ31 substrate, steam coating, SC/BTESPT and SC/BTESPT/Ce^{3+} hybrid coatings after immersion for 240 h

is the lowest. The HERs (Figs. 9(b, b′)) can be arranged in the following ascending order: SC/BTESPT/Ce^{3+} < SC/BTESPT < steam coating < the substrate, indicating a good resistance for the hybrid coatings. The initial decrease in the HER for the AZ31 alloy is related to the dissolution of substrate and the formation of $Mg(OH)_2$ precipitate. Particularly, the fluctuation of the HER of the steam coating may be caused by the self-healing ability of the LDH. The HER results of the hybrid coatings are close to zero during the whole immersion process which may be due to the better barrier properties of BTESPT and $Ce(NO_3)_3$, which can effectively protect the substrate. As can be seen, the HER of the SC/BTESPT/Ce^{3+} coating is the lowest during the whole immersion period, implying a better protection to the substrate.

Figure 10 shows the SEM images of the samples after immersion for 240 h in 3.5 wt.% NaCl solution. It can be clearly seen from Fig. 10(a) that the surface of the AZ31 alloy is severely damaged after immersion. As can be seen from Fig. 10(b), compared with the original sample, the morphology of the steam coating after immersion changed drastically, the nano-plate structure of LDH disappeared and the surface had cracks. Figures 10(c) and (d) show the SEM images of SC/BTESPT coating and SC/BTESPT/Ce^{3+} coating, respectively, which have similar structures. Compared with the original sample, the oily substance began to disappear, and the nano-plate structure of LDH was retained. In addition, there are no significant cracks on the surface of the hybrid coating, indicating that the coating is more stable than other samples.

The elemental compositions of samples after immersion in 3.5 wt.% NaCl solution for 240 h are shown in Fig. 11. Points 1, 2, 3 and 4 in Fig. 10 correspond to AZ31 substrate, steam coating, SC/BTESPT coating and SC/BTESPT/Ce^{3+} coating. It is noted that there are a great proportion of O and Mg elements for all the samples, indicating that $Mg(OH)_2$ may be formed as the corrosion product. The concentration of Al in the steam coating is the highest, which may be due to the corrosion of magnesium in preference to aluminum during corrosion. The concentrations of S and Si elements have a great difference for the hybrid coatings. The content of S and Si elements of SC/BTESPT/Ce^{3+} coating was higher than that of SC/BTESPT coating, which demonstrated that the SC/BTESPT/Ce^{3+} coating is relatively stable and compact compared with the SC/BTESPT coating. It is worth noting that no Ce element was detected after the immersion, which may be due to the corrosion of the coating in the presence of Ce.

XRD patterns of steam coating and hybrid coatings after immersion are shown in Fig. 12. As a

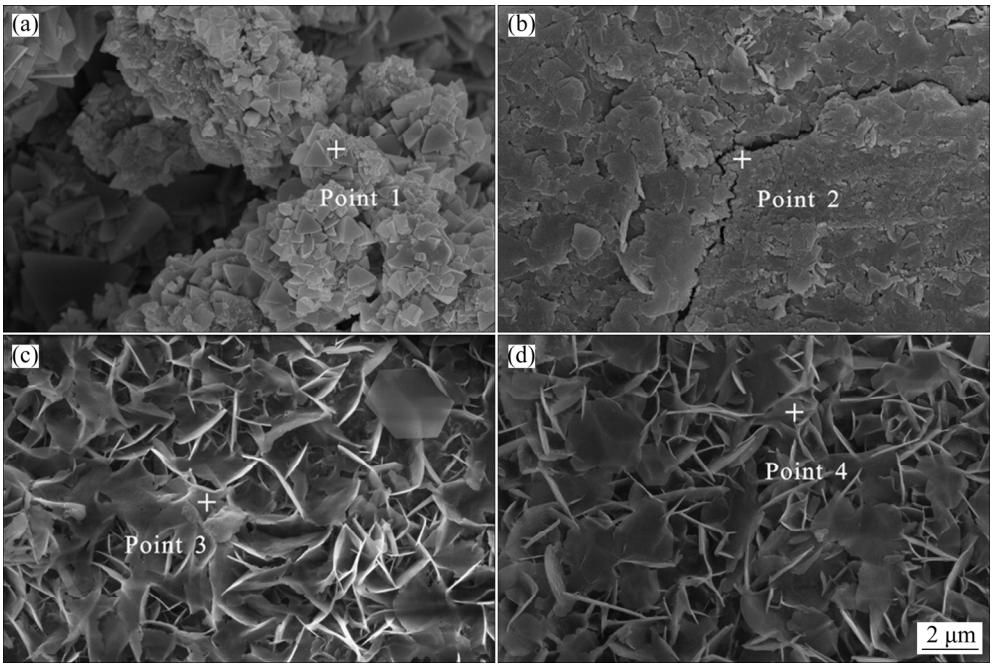

Fig. 10 SEM images of AZ31 substrate (a), steam coating (b), SC/BTESPT coating (c) and SC/BTESPT/Ce^{3+} coating (d) after immersion in 3.5 wt.% NaCl solution for 240 h

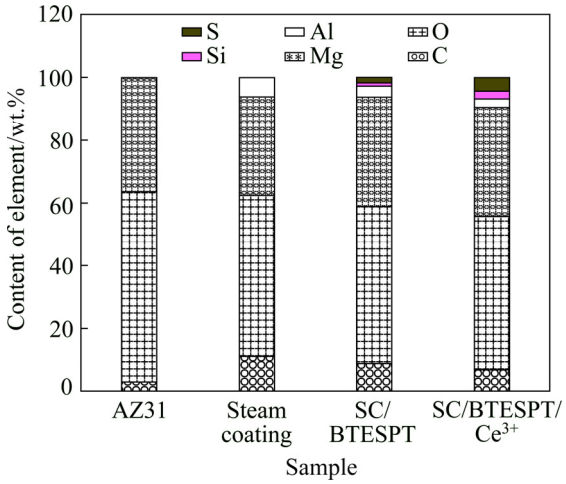

Fig. 11 Elemental compositions of AZ31 substrate, steam coating and hybrid coatings after immersion for 240 h (Points 1, 2, 3 and 4 in Fig. 10)

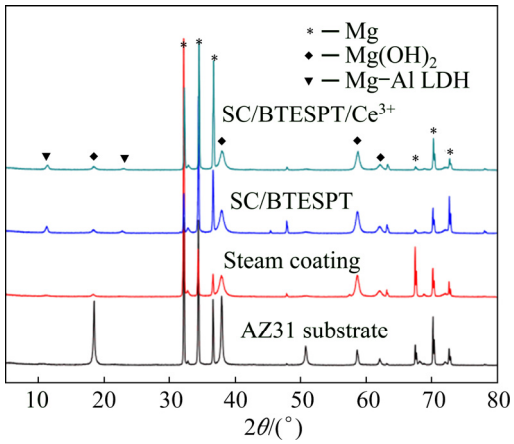

Fig. 12 XRD patterns of steam coating and hybrid coatings after immersion in 3.5 wt.% NaCl solution for 240 h

corrosion product, the characteristic peaks of $Mg(OH)_2$ are at 18.4°, 37.9° and 58.6° on all coating. It is noted that the two peaks at 11.3° and 22.6° in the steam coating and all hybrid coatings can be designated as diffraction of LDH peak. It is proved that the steam coating is not completely corroded, suggesting a stable structure of the as-prepared coatings.

4 Discussion

4.1 Comparison in coatings on Mg alloys

At present, there are many methods for preparing LDH coatings, most of them are prepared by two-step method [43], which is complicated and requires a lot of time. Here, we adopted a simple, time-saving one-step in-situ steam coating method to prepare a LDH coating on the surface of AZ31 magnesium alloy, and it had good corrosion resistance. In addition, we used a good silane coupling agent (BTESPT) to modify the LDH steam coating, and added a small amount of $Ce(NO_3)_3$ to enhance the performance of the silane coating, which had a significant effect. The SC/BTESPT/Ce^{3+} hybrid coating had a very low self-corrosion current density, and still protected the substrate well after immersion for 240 h.

4.2 Coating formation mechanism

Based on the above results, in a closed reaction vessel, the steam produced at high pressure and temperature would have a high kinetic energy and reactivity, thus steam can react with dissolved Mg^{2+} and Al^{3+} ions in magnesium alloys, resulting in the formation of carbonate Mg−Al LDH and $Mg(OH)_2$. When BTESPT was coated on the steam coating, a hydrolysis reaction (Reaction 1) occurred to obtain a $(OH)_3Si(CH_2)_3S_4(CH_2)_3(OH)_3$ group, then the group reacted with the Mg—OH groups of the steam coating, which was via hydrolysis condensation reactions shown in Reaction (2). In addition, self-condensation (Reaction 3) of Si—OH groups also occurred [43]. Therefore, after silane is hydrolyzed, Si—O—Mg is formed by chemical reaction to bond with the steam coating, and silane can also form a network structure of Si—O—Si to cover the coating surface.

$$(H_5C_2O)_3Si(CH_2)_3S_4(CH_2)_3Si(OC_2H_5)_3+3H_2O\rightarrow (OH)_3Si(CH_2)_3S_4(CH_2)_3Si(OH)_3+3H_5C_2OH \quad (1)$$

$$Mg—OH+Si—OH\rightarrow Si—O—Mg+H_2O \quad (2)$$

$$2Si—OH\rightarrow Si—O—Si+H_2O \quad (3)$$

4.3 Corrosion mechanism

When the hybrid coating was immersed in 3.5 wt.% NaCl solution, H_2O and Cl^- were harmful to the coated sample. As a result, the hybrid coating began to corrode (Fig. 13(b)). As the immersion time increased, corrosion occurred on the surface of the magnesium substrate, which will lead to the generation of hydrogen and local bubbling, causing the BTESPT coating to expand and fall off (Fig. 13(c)), which also rendered that the steam coating was completely exposed. Subsequently, the steam coating was more severely damaged (Fig. 13(d)).

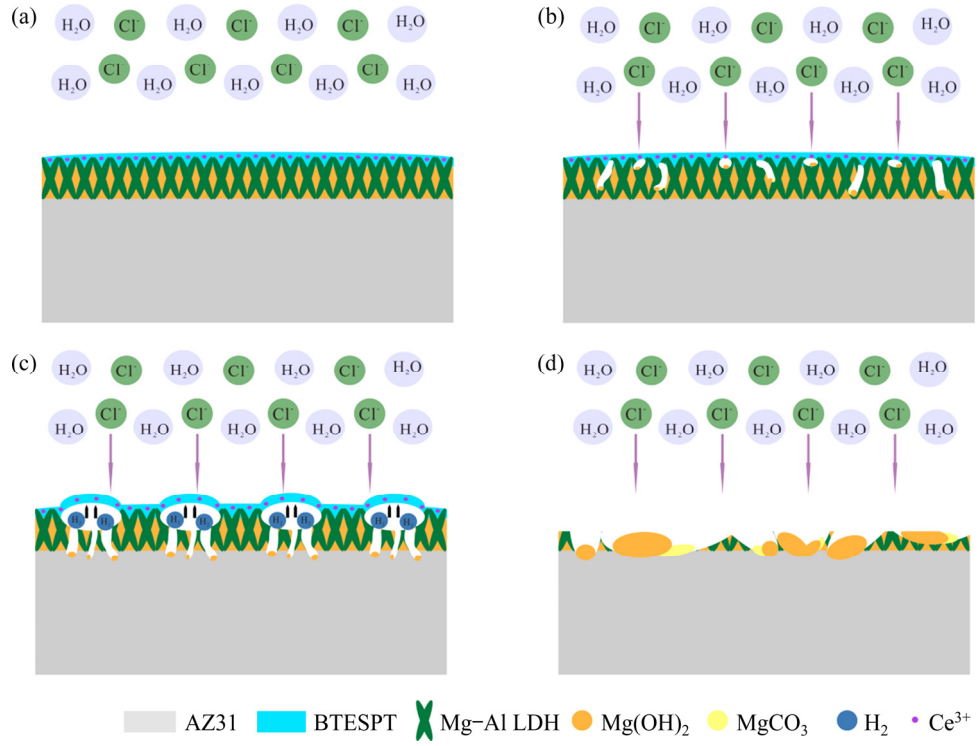

Fig. 13 Schematic representation of SC/BTESPT/Ce^{3+} coating (a) and its corrosion mechanism (b, c, d)

When LDH coating was exposed to 3.5 wt.% NaCl solution, the anion-exchange reaction would happen, and Reaction (4) is as follows:

$$MgAl—CO_3^{2-}—LDH+2Cl^-\rightarrow MgAl—2Cl^-—LDH+CO_3^{2-} \quad (4)$$

At the same time, the self-healing reaction to form $Mg(OH)_2$ and the subsequent corrosion reaction are shown as

$$Mg^{2+}+CO_3^{2-}\rightarrow MgCO_3\downarrow \quad (5)$$

$$MgCO_3+2OH^-\rightarrow Mg(OH)_2\downarrow+CO_3^{2-} \quad (6)$$

$$Mg(OH)_2+2Cl^-\rightarrow MgCl_2+2OH^- \quad (7)$$

Finally, electrochemical corrosion occurs when the medium solution enters the substrate through the pores of the vapor coating. The reaction is shown as

$$Mg+2H_2O\rightarrow Mg(OH)_2\downarrow+H_2\uparrow \quad (8)$$

The enhanced volume resulted from the formation of $Mg(OH)_2$ and H_2, which further led to the dissolution of the BTESPT coating.

5 Conclusions

(1) The SC/BTESPT and SC/BTESPT/Ce^{3+} coatings were prepared on the surface of AZ31 Mg alloy by combining an in-situ steam growth process and a subsequent immersion treatment. The immersion test demonstrated that the SC/BTESPT/Ce^{3+} coatings can provide a long-term corrosion protection for the AZ31 alloy.

(2) As a dopant, Ce^{3+} can effectively improve the corrosion resistance of BTESPT coating. Corrosion current density of SC/BTESPT hybrid coating decreased by three orders of magnitude compared with the AZ31 substrate. The hydrogen evolution rate of SC/BTESPT/Ce^{3+} hybrid coating was the lowest after 240 h of immersion, indicating that SC/BTESPT/Ce^{3+} coatings possessed a good corrosion resistance.

(3) The silane is combined with steam coating through chemical reaction, the addition of $Ce(NO_3)_3$ can promote the hydrolysis and agglomeration of the silane, making the hybrid coating more stable, and the LDH has the self-healing function, which lead to good corrosion resistance of the hybrid coating.

References

[1] DING Z Y, CUI L Y, CHEN X B, ZENG R C, GUAN S K, LI S Q, ZHANG F, ZOU Y H, LIU Q Y. In vitro corrosion of micro-arc oxidation coating on Mg−1Li−1Ca alloy: The influence of intermetallic compound Mg_2Ca [J]. Journal of

Alloys and Compounds, 2018, 764: 250−260.

[2] CHENG Y F, DU W B, LIU K, FU J J, WANG Z H, LI S B, FU J L. Mechanical properties and corrosion behaviors of Mg−4Zn−0.2Mn−0.2Ca alloy after long term in vitro degradation [J]. Transactions of Nonferrous Metals Society of China, 2020, 30: 363−372.

[3] BAGHANI A, KHALILPOUR H, MIRESMAEILI S M. Microstructural evolution and creep properties of Mg−4Sn alloys by addition of calcium up to 4 wt.% [J]. Transactions of Nonferrous Metals Society of China, 2020, 30: 896−904.

[4] WU W, ZHANG F, LI Y C, SONG L, JIANG D, ZENG R C. Corrosion resistance of dodecanethiol-modified magnesium hydroxide coating on AZ31 magnesium alloy [J]. Applied Physics A—Materials Science & Processing, 2020, 126: 8.

[5] ZHANG G, WU L, TANG A T, WENG B, ATRENS A, MA S D, LIU L, PAN F S. Sealing of anodized magnesium alloy AZ31 with MgAl layered double hydroxides layers [J]. RSC Advances, 2018, 8: 2248−2259.

[6] BAGHERI B, ABBASI M, ABDOLLAHZADEH A, MIRSALEHI S E. Effect of second-phase particle size and presence of vibration on AZ91/SiC surface composite layer produced by FSP [J]. Transactions of Nonferrous Metals Society of China, 2020, 30: 905−916.

[7] PRABHU D B, GOPALAKRISHNAN P, RAVI K R. Morphological studies on the development of chemical conversion coating on surface of Mg−4Zn alloy and its corrosion and bio mineralisation behaviour in simulated body fluid [J]. Journal of Alloys and Compounds, 2020, 812: 152146.

[8] FAN X L, HUO Y F, LI C Y, KANNAN M B, CHEN X B, GUAN S K, ZENG R C, MA Q L. Corrosion resistance of nanostructured magnesium hydroxide coating on magnesium alloy AZ31: Influence of EDTA [J]. Rare Metals, 2019, 38: 520−531.

[9] TENG Y X, LIU F, LI C Y, XU Z, GUO J. Fabrication and degradation properties of Ca/P contained micro-arc oxidation coating on pure magnesium [J]. Science of Advanced Materials, 2020, 12: 755−759.

[10] LI C Y, FAN X L, ZENG R C, CUI L Y, LI S Q, ZHANG F, HE Q K, KANNAN M B, JIANG H W, CHEN D C, GUAN S K. Corrosion resistance of in-situ growth of nano-sized $Mg(OH)_2$ on micro-arc oxidized magnesium alloy AZ31: Influence of EDTA [J]. Journal of Materials Science & Technology, 2019, 35: 1088−1098.

[11] JIN T, HAN Y Q, BAI R Q, LIU X. Corrosion protection properties of nano NH_2-reduced graphene oxide/epoxy composite coatings formed by self-curing on magnesium alloy [J]. Journal of Nanoscience and Nanotechnology, 2018, 18: 4971−4981.

[12] SHEN S Y, ZUO Y. The improved performance of Mg-rich epoxy primer on AZ91D magnesium alloy by addition of ZnO [J]. Corrosion Science, 2014, 87: 167−178.

[13] CHEN X B, YANG H Y, ABBOTT T B, EASTON M A, BIRBILIS N. Corrosion resistant electrochemical platings on magnesium alloys: A state-of-the-art review [J]. Corrosion, 2012, 68: 518−535.

[14] SINGH C, TIWARI S K, SINGH R. Exploring environment friendly nickel electrodeposition on AZ91 magnesium alloy: Effect of prior surface treatments and temperature of the bath on corrosion behaviour [J]. Corrosion Science, 2019, 151: 1−19.

[15] ZHOU M, YAN L C, LING H, DIAO Y P, PANG X L, WANG Y L, GAO K W. Design and fabrication of enhanced corrosion resistance Zn−Al layered double hydroxides films based anion-exchange mechanism on magnesium alloys [J]. Applied Surface Science, 2017, 404: 246−253.

[16] ZHANG G, WU L, TANG A T, MA Y L, SONG G L, ZHENG D J, JIANG B, ATRENS A, PAN F S. Active corrosion protection by a smart coating based on a MgAl-layered double hydroxide on a cerium-modified plasma electrolytic oxidation coating on Mg alloy AZ31 [J]. Corrosion Science, 2018, 139: 370−382.

[17] ZHANG G, WU L, TANG A, ZHANG S, YUAN B, ZHENG Z, PAN F. A novel approach to fabricate protective layered double hydroxide films on the surface of anodized Mg−Al alloy [J]. Advanced Materials Interfaces, 2017, 4: 1700163.

[18] CHEN J, SONG Y, SHAN D, HAN E H. Study of the corrosion mechanism of the in situ grown Mg−Al−CO_3^{2-} hydrotalcite film on AZ31 alloy [J]. Corrosion Science, 2012, 65: 268−277.

[19] LIU L, WU L, CHEN X B, SUN D E, CHEN Y, ZHANG G, DING X X, PAN F S. Enhanced protective coatings on Ti−10V−2Fe−3Al alloy through anodizing and post-sealing with layered double hydroxides [J]. Journal of Materials Science & Technology, 2020, 37: 104−113.

[20] ZHAO M Q, ZHANG Q, HUANG J Q, WEI F. Hierarchical nanocomposites derived from nanocarbons and layered double hydroxides: Properties, synthesis, and applications [J]. Advanced Functional Materials, 2012, 22: 675−694.

[21] YE X, JIANG Z M, LI L X, XIE Z H. In-Situ Growth of NiAl-layered double hydroxide on AZ31 Mg alloy towards enhanced corrosion protection [J]. Nanomaterials, 2018, 8: 411.

[22] WU L, YANG D N, ZHANG G, ZHANG Z, ZHANG S, TANG A T, PAN F S. Fabrication and characterization of Mg−M layered double hydroxide films on anodized magnesium alloy AZ31 [J]. Applied Surface Science, 2018, 431: 177−186.

[23] YAO Q S, LI Z C, QIU Z M, ZHANG F, CHEN X B, CHEN D C, GUAN S K, ZENG R C. Corrosion resistance of $Mg(OH)_2$/Mg−Al-layered double hydroxide coatings on magnesium alloy AZ31: Influence of hydrolysis degree of silane [J]. Rare Metals, 2019, 38: 629−641.

[24] ZENG R C, LI X T, LIU Z G, ZHANG F, LI S Q, CUI H Z. Corrosion resistance of Zn−Al layered double hydroxide/poly(lactic acid) composite coating on magnesium alloy AZ31 [J]. Frontiers of Materials Science, 2015, 9: 355−365.

[25] ZENG R C, LIU Z G, ZHANG F, LI S Q, CUI H Z, HAN E H. Corrosion of molybdate intercalated hydrotalcite coating on AZ31 Mg alloy [J]. Journal of Materials Chemistry A, 2014, 2: 13049−13057.

[26] KAMIYAMA N, PANOMSUWAN G, YAMAMOTO E, SUDARE T, SAITO N, ISHIZAKI T. Effect of treatment time in the $Mg(OH)_2$/Mg−Al LDH composite film formed on Mg alloy AZ31 by steam coating on the corrosion resistance [J]. Surface & Coatings Technology, 2016, 286: 172−177.

[27] ISHIZAKI T, CHIBA S, SUZUKI H. In situ formation of anticorrosive Mg−Al layered double hydroxide-containing magnesium hydroxide film on magnesium alloy by steam

coating [J]. ECS Electrochemistry Letters, 2013, 2: 15−17.
[28] ISHIZAKI T, CHIBA S, WATANABE K, SUZUKI H. Corrosion resistance of Mg−Al layered double hydroxide container-containing magnesium hydroxide films formed directly on magnesium alloy by chemical-free steam coating [J]. Journal of Materials Chemistry A, 2013, 1: 8968−8977.
[29] QIAO L Y, LAI N, LI W, WANG Y, WANG W L. Structure and corrosion performance of silane/sodium hyaluronate composite coating on pure magnesium [J]. Rare Metal Materials and Engineering, 2020, 49: 304−312.
[30] TOORANI M, ALIOFKHAZRAEI M, MAHDAVIAN M, NADERI R. Effective PEO/Silane pretreatment of epoxy coating applied on AZ31B Mg alloy for corrosion protection [J]. Corrosion Science, 2020, 169: 108608.
[31] NAJIBZAD A S, AMINI R, ROSTAMI M, KARDAR P, FEDEL M. Active corrosion performance of magnesium by silane coatings reinforced with polyaniline/praseodymium [J]. Progress in Organic Coatings, 2020, 140: 105504.
[32] ZHANG Z Q, ZENG R C, LIN C G, WANG L, CHEN X B, CHEN D C. Corrosion resistance of self-cleaning silane/polypropylene composite coatings on magnesium alloy AZ31 [J]. Journal of Materials Science & Technology, 2020, 41: 43−55.
[33] ZENG R C, ZHANG F, LAN Z D, CUI H Z, HAN E H. Corrosion resistance of calcium-modified zinc phosphate conversion coatings on magnesium–aluminium alloys [J]. Corrosion Science, 2014, 88: 452−459.
[34] YAO Q S, ZHANG F, SONG L, ZENG R C, CUI L Y, LI S Q, WANG Z L, HAN E H. Corrosion resistance of a ceria/polymethyltrimethoxysilane modified Mg−Al-layered double hydroxide on AZ31 magnesium alloy [J]. Journal of Alloys and Compounds, 2018, 764: 913−928.
[35] HOU L F, LI Y L, SUN J L, ZHANG S H, WEI H, WEI Y H. Enhancement corrosion resistance of Mg−Al layered double hydroxides films by anion-exchange mechanism on magnesium alloys [J]. Applied Surface Science, 2019, 487: 101−108.
[36] CHEN J, SONG Y, SHAN D, HAN E H. Influence of alloying elements and microstructure on the formation of hydrotalcite film on Mg alloys [J]. Corrosion Science, 2015, 93: 90−99.
[37] DING P, LI Z Z, WANG Q, ZHANG X J, TANG S F, SONG N, SHI L Y. In situ growth of layered double hydroxide films under dynamic processes: Influence of metal cations [J]. Materials Letters, 2012, 77: 1−3.
[38] OZTURK S, BALKOSE D, OKUR S, UMEMURA J. Effect of humidity on electrical conductivity of zinc stearate nanofilms [J]. Colloids & Surfaces A: Physicochemical & Engineering Aspects, 2007, 302: 67−74.
[39] WOJCIECHOWSKI J, SZUBERT K, PEIPMANN R, FRITZ M, SCHMIDT U, BUND A, LOTA G. Anti-corrosive properties of silane coatings deposited on anodised aluminium [J]. Electrochim Acta, 2016, 220: 1−10.
[40] WANG Y, GU Z, LIU J, JIANG J, YUAN N, PU J, DING J. An organic/inorganic composite multi-layer coating to improve the corrosion resistance of AZ31B Mg alloy [J]. Surface and Coatings Technology, 2019, 360: 276−284.
[41] WANG Y, GU Z, YUAN N, PU J, DING J. Fabrication of anticorrosion dual-component silane film on AZ31 Mg alloy surface by self-assembly method [J]. JOM, 2019, 2: 730−737.
[42] ZHANG F, LIU Z G, ZENG R C, LI S Q, CUI H Z, SONG L, HAN E H. Corrosion resistance of Mg−Al-LDH coating on magnesium alloy AZ31 [J]. Surface & Coatings Technology, 2014, 258: 1152−1158.
[43] DOU B, WANG Y, ZHANG T, MENG G, SHAO Y, LIN X, WANG F. Electrochemically assisted silanization treatment of an aluminum alloy under oxygen pressure for corrosion protection [J]. New Journal of Chemistry, 2018, 42: 9771−9782.

AZ31 镁合金上 Mg−Al LDH/$Mg(OH)_2$/硅烷−Ce 杂化涂层的耐蚀性

仇在孟[1]，曾荣昌[1,2]，张 芬[1]，宋 亮[1]，李硕琦[1]

1. 山东科技大学 材料科学与工程学院 轻金属腐蚀实验室，青岛 266590；
2. 郑州大学 材料科学与工程学院，郑州 450002

摘 要：在 AZ31 镁合金基体上涂覆一种环保杂化涂层。通过原位蒸汽涂覆工艺制备 Mg−Al 层状双氢氧化物 Mg−Al LDH/$Mg(OH)_2$ 涂层，随后使用双-[三乙氧基甲硅烷基丙基]四硫化物(BTESPT)硅烷和 $Ce(NO_3)_3$ 对蒸汽涂层进行表面改性，研究两者对 AZ31 镁合金的协同作用。通过 X 射线衍射仪(XRD)、扫描电子显微术(SEM)、傅里叶变换红外光谱(FT-IR)和 X 射线光电子能谱(XPS)研究杂化涂层的显微结构和组成特征。通过电位动力学极化(PDP)、电化学阻抗谱(EIS)和浸入 3.5 wt.% NaCl 溶液中的析氢速率评价涂层样品的耐蚀性。结果表明，在 BTESPT 硅烷和 $Ce(NO_3)_3$ 存在下，合金的耐蚀性得到改善，这很可能是由于蒸汽涂层和硅烷涂层的协同作用增强了杂化涂层的阻隔性能。此外，还讨论涂层的形成机理和耐蚀机理。

关键词：镁合金；硅烷涂层；层状双氢氧化物；耐蚀性

(Edited by Xiang-qun LI)